Acta Mech
https://doi.org/10.1007/s00707-024-04072-0

ORIGINAL PAPER

**Ata Alipour Ghassabi · Ali Razgordanisharahi · Gullu Kiziltas Sendur · Yaser Kiani · Christian Hellmich**

# An exact analytical method for free vibration analysis of FG-GPLRC sector cylindrical shells under Levy-type boundary conditions

Received: 3 March 2024 / Revised: 7 May 2024 / Accepted: 11 August 2024


**Abstract** In this article, an exact analytical method for the free vibration analysis of functionally graded (FG) graphene platelet (GPL)-reinforced composite (GPLRC) sector cylindrical shells is presented by considering Levy-type boundary conditions for the first time. The analysis relies on the use of the Halpin–Tsai micro-mechanical model for evaluating the material properties of the graded layers of the shell with three different grading patterns. Mathematical modeling of the Levy-type cylindrical shell is based on the Hamilton principle and the Sanders first-order shear deformation theory (FSDT). The governing equations of the composite shell are analytically solved using the state-space method. The validity of the proposed analytical method is demonstrated by the excellent agreement between the obtained results of the exact analytical solution and the results available in the literature. Furthermore, some parametric studies are conducted to reveal the effects of variations in boundary conditions, GPL distribution patterns, GPL weight fraction, and geometrical parameters such as shallowness angle, length-to-radius ratio, and thickness on the free vibration behavior of the shell structure. Natural frequencies and mode switching are reported for different mode numbers.

## Abbreviations

| | |
|---|---|
| C | Clamped boundary |
| CNT | Carbon nanotubes |
| F | Free boundary |
| FEM | Finite element method |
| FG | Functionally graded |
| FSDT | First-order shear deformation theory |
| GPL | Graphene platelet |
| ODE | Ordinary differential equation |
| RC | Reinforced composite |

A. A. Ghassabi (✉) · G. K. Sendur
Faculty of Engineering and Natural Sciences, Sabanci University, Istanbul, Turkey
E-mail: ata.alipour@sabanciuniv.edu

A. Razgordanisharahi (✉) · C. Hellmich
Institute for Mechanics of Materials and Structures, TU Wien - Vienna University of Technology, Vienna, Austria
E-mail: ali.razgordanisharahi@tuwien.ac.at

Y. Kiani
Faculty of Engineering, Shahrekord University, Shahrekord, Iran

Y. Kiani
Nanotechnology Research Institute, Shahrekord University, Shahrekord, Iran

Published online: 09 September 2024

| | |
|---|---|
| S | Simply supported boundary |

**List of symbols**

| | |
|---|---|
| $\eta_L$ | Auxiliary coefficient |
| $\eta_T$ | Auxiliary coefficient |
| $\nu^{(k)}$ | Effective Poisson's ratio of the $k$-th layer |
| $\omega_m$ | Natural frequency of the $m$-th vibrating mode |
| $\psi$ | Rotation of middle surface of the panel |
| $\rho^{(k)}$ | Effective mass density of the $k$-th layer |
| $\rho_{\mathrm{GPL}}$ | Mass density of GPLs |
| $\rho_{\mathrm{m}}$ | Mass density of polymer matrix |
| $\theta$ | Central angle of the panel |
| $\xi_L$ | Geometrical coefficient |
| $\xi_T$ | Geometrical coefficient |
| $a_{\mathrm{GPL}}$ | Average GPL length |
| $b$ | Panel side length |
| $b_{\mathrm{GPL}}$ | Average GPL width |
| $E$ | Young's modulus |
| $E^{(k)}$ | Effective elastic modulus of the $k$-th layer |
| $E_{\mathrm{m}}$ | Elastic modulus of the polymer matrix |
| $E_{\mathrm{GPL}}$ | Elastic modulus of the GPLs |
| $h$ | Total thickness |
| $I_{\mathrm{i}}$ | Inertia |
| $k_{\mathrm{s}}$ | Shear correction factor |
| $L$ | Panel length |
| $m$ | Number of half-waves in circumferential direction |
| $M_i$ | Bending moment |
| $n$ | Number of half-waves in axial direction |
| $N_i$ | Normal force |
| $N_L$ | Stratification number |
| $Q_i$ | Shear force |
| $Q_{ij}^{(k)}$ | Elements of material stiffness matrix |
| $R$ | Radius of curvature |
| $t$ | Time |
| $t_{\mathrm{GPL}}$ | Average GPL thickness |
| $u$ | Displacement of a point on the middle surface in $x_1$ direction |
| $v$ | Displacement of a point on the middle surface in $x_2$ direction |
| $V_m^{(k)}$ | Polymer matrix volume fraction of the $k$-th layer |
| $V_{\mathrm{GPL}}^{*}$ | Total GPL volume fraction |
| $V_{\mathrm{GPL}}^{(k)}$ | GPL volume fraction of the $k$-th layer |
| $w$ | Displacement of a point on the middle surface in $z$ direction |
| $W_{\mathrm{GPL}}$ | Mean weight fraction of GPLs |

## 1 Introduction

Nanocomposite technology is an emergent area of study wherein nanofillers are incorporated into a polymer matrix to enhance their mechanical, optical, thermal, and electrical properties and introduce innovative characteristics. According to the method of reinforcement, nanocomposites can be divided into fibrous, laminar, and particulate nanocomposites [1]. Currently, a wide range of nanofillers are utilized in nanocomposites, with the cost and availability of these fillers undergoing constant fluctuations owing to the nascent nature of the field and the continued development of such fillers. Nanofillers like carbon nanotubes (CNT), graphene oxide, and graphene platelets are the most commonly used reinforcements in theory and practice. The particle–matrix interaction results in remarkable property enhancements, enabling these materials to compete technically and

commercially with their conventional counterparts [2]. Graphene, which is grown in various forms, including graphene nanosheets and graphene nanoplatelets, is a carbon nanoallotrope with a hexagonal honeycomb nanostructure. Various morphologies of graphene have given rise to a wide range of physical and chemical properties, such as exceptional electrical, thermal, and mechanical features. A noteworthy carbon nanomaterial is the graphene nanoplatelet. This specific configuration of graphene comprises a cluster of graphene nanosheets that possess an outstanding specific surface area and exhibit remarkable electrical, thermal, and mechanical characteristics. Graphene nanoplatelets can interact with polymers, therefore improving the thermal, electrical, and mechanical characteristics of the resulting GPLRC structures. As a result of these impressive properties, these nanocomposites have found significant applications in numerous disciplines of science and engineering [3]. Several studies on the linear and nonlinear free and forced vibrations of different FG-GPLRC nanocomposites are described below.

Kitipornchai et al. [4] analyzed the free vibration of FG-GPLRC porous beams based on the Timoshenko beam theory and Ritz method. Symmetric porosity and GPL distribution patterns proved to be the most effective in improving the stiffness of the structure. Jafari et al. [5] presented a four-variable shear and normal deformable quasi-3D beam model to analyze the free and forced vibrations of FG-GPLRC beams under moving loads. Feng et al. [6] numerically explored the nonlinear free vibration of FG-GPLRC beams with different boundary conditions using the Ritz method. Bahranifard et al. [7] scrutinized the in-plane vibrational characteristics of curved beams composed of multilayer FG-GPLRC material within a thermally influenced environment and under the effect of dynamic moving loads. A multiscale numerical approach was proposed by Zhang et al. [8] to study the static behavior, dynamic response, and stability of FG-GPLRC beams under various boundary conditions. Several studies available in the literature investigated the vibration behavior of FG-GPLRC plates with different geometries [9–11]. Based on the nonlocal strain gradient theory, vibration responses of small-scale FG-GPLRC plates were analyzed using exponential shear deformation plate theory [12] and Kirchhoff plate model [13]. Different solution techniques, including Chebyshev–Ritz [14], isogeometric [15], mesh-free [16], and spectral Chebyshev [17] approaches, were employed by researchers to compute the frequency characteristics of FG-GPLRC plates. Additionally, Muni Rami Reddy et al. [18] presented a finite element model based on the first-order shear deformation theory to obtain the natural frequencies of FG-GPLRC plates under various boundary conditions.

Shell structures play a pivotal role in engineering designs due to their widespread use in a variety of structural applications. Essentially, a shell structure is a three-dimensional geometry that is thin in one direction when compared with the other two dimensions. This unique geometric configuration renders them thin and lightweight and allows them to span large areas. Common applications of shell structures include the construction of expansive roofs in civil engineering, their incorporation into car bodies within the automobile industry, integration into aircraft bodies and rockets in aeronautical engineering, and utilization in the hulls of ships and submarines in naval architecture. A specific sub-type of shell is the cylindrical shell, which finds extensive use in aerospace and naval construction. Cylindrical shells often serve as load-bearing structures for aircraft, rockets, and submarines. In these applications, the cylindrical shells are typically reinforced to enhance strength, stiffness, and buckling resistance [19]. The natural frequencies of cylindrical shells are closely grouped in a narrow band, making them susceptible to resonant vibrations. To manage and control the amplitudes of these vibrations, understanding the distribution of natural frequencies is crucial to avoiding failure under dynamic loads in operation. Also, the accuracy of the vibration analysis in an exact analytical and realistic setting such as the one presented in the paper will allow for the correct determination of the dynamic response under different operating conditions represented by a variety of different boundary conditions presented here [20]. Numerous studies in the literature are dedicated to the vibration analysis of FG-GPLRC shells with different geometries. Safarpour et al. [21] exploited the differential quadrature method to analyze free vibrations of the FG-GPLRC truncated conical shell, cylindrical shell, and annular plate based on the three-dimensional elasticity theory. The effects of rotational springs on the edges [22], pressure and thermal environment [23], magneto-electro-elastic face sheets [24], piezoelectric face sheets [25], fluid–structure interaction [26], and size dependency [27] on vibration behavior of FG-GPLRC shells were also examined in open literature. NURBS-based [28], Bezier extraction-based [29], and B-spline-based [30] isogeometric analyses were reported for the vibration characteristics of FG-GPLRC shells with various shapes. Based on the Navier solution method and Donnell kinematic relationships, Baghbadorani et al. [31] studied free vibrations of first-order shear deformable FG-GPLRC cylindrical shells. Studies on free vibration of FG-GPLRC cylindrical shells with initial stresses [32] and resting on elastic foundations [33] were also reported. Natural frequencies of FG-GPLRC doubly curved shells with simply supported [34] and arbitrary [35] edge supports were obtained using the Navier and

Ritz methods, respectively. Qin et al. [36] proposed a unified solution for analyzing the vibration behavior of GPL-reinforced laminated shallow shells using the Rayleigh–Ritz method and the artificial spring technique.

According to the above literature survey, the free vibration of FG-GPLRC beams and plates has been widely studied by different researchers over the years. Contrary to the extensive research on beam and plate structures, the number of studies that examine the behavior of shell structures remains limited, with the majority of those focusing on FG-GPLRC cylindrical shell geometries being limited to closed full cylindrical shells. To the best of the authors' knowledge, the most relevant study in the literature that examines open sector cylindrical shells made of GPL-reinforced composites is the work by Wang et al. [34], which exclusively addresses the problem solution for simply supported (SSSS) FG-GPLRC open cylindrical shells using Navier's approach. Unlike existing studies, here we present for the first time an exact analytical solution for the vibration behavior of open sector cylindrical shells made of GPL-reinforced functionally graded material. This study stands out with a proposed solution for the governing equations of motion under Levy-type boundary conditions, extending the applicability of solutions for possible combinations of support types on four edges of the shell structure, namely SCSC, SCSS, SSSS, SCSF, SSSF, and SFSF. As another novel feature of the proposed exact analytical scheme, mode switching is reported, which allows for practical implications in real-life applications of such structures. The analytical procedure relies on the state-space Levy method, a robust analytical technique grounded in the state-space concept, providing exact Levy-type solutions. This method proves particularly advantageous when analyzing structures with shear deformation theories, where the number of governing partial differential equations exceeds that of classical theories. Unlike some of the well-known numerical approaches, the presented exact analytical approach stands out by eliminating the need for classical discretization and totally avoiding the inherent challenges, errors, and approximations of the numerical methods. Shear locking and hourglassing are examples of typical challenges in the finite element approach that can be eliminated by using analytical schemes. Compared to other analytical approaches such as Navier's solution method, which can only accommodate simply supported boundaries on all edges, the proposed method excels in addressing different combinations of Levy-type boundary conditions. The requirement of two simply supported parallel edges is the only limitation of this analytical solution procedure compared to widely used numerical schemes such as the finite element method. Nevertheless, the presented procedure allows for the representation of a wide range of different boundary conditions applicable to practical engineering problems in a computationally efficient and accurate manner, surpassing the performance of most numerical methods. The first-order shear deformation theory and the assumptions of Sanders are adopted for the mathematical modeling of the shell structure. It is important to note that the assumptions made for all the multilayered functionally graded structures discussed in this paper include the dispersion of fillers in each individual layer in a random and uniform manner with perfect bonding. Additionally, there is an assumption of no jump conditions in fields, as well as no delamination or debonding across neighboring layers within the laminated structures [37]. Through some parametric studies, the influence of GPL weight fraction, stratification number, GPL distribution pattern, shallowness angle, and other geometrical parameters on the natural frequencies of the structure is examined. The natural frequencies and mode switching phenomenon are reported for different mode numbers and boundary conditions.

## 2 Material properties

A GPLRC cylindrical shell with constant thickness $h$, side lengths $L$ and $b$, and radius of curvature $R$ is presented in Fig. 1. The functionally graded cylindrical shell consists of $N_L$ number of GPLRC layers of the same thickness. In each ply of thickness $h/N_L$, the isotropic polymer matrix is reinforced by GPLs. The weight fraction of GPLs is varied according to three symmetric patterns, namely FG-U, FG-X, and FG-O [37]. A cylindrical shell made of GPLRC layers in the FG-U pattern has a uniform weight fraction of GPLs along the thickness direction. For FG-X composites, the top and bottom plies of the shell are GPL rich, whereas more GPLs are embedded in the middle layers of FG-O laminates. The volume fraction of GPLs for the $k$-th layer of the FG composite shell can be calculated by

$$\begin{aligned}
&\text{U - GPLRC: } V_{\mathrm{GPL}}^{(k)} = V_{\mathrm{GPL}}^{*} \\
&\text{X-GPLRC: } V_{\mathrm{GPL}}^{(k)} = 2V_{\mathrm{GPL}}^{*} \left|2k - N_L - 1\right| / N_L \\
&\text{O - GPLRC: } V_{\mathrm{GPL}}^{(k)} = 2V_{\mathrm{GPL}}^{*} \left(1 - \left|2k - N_{\mathrm{L}} - 1\right| / N_L\right)
\end{aligned} \tag{1}$$

where $k$ ranges from 1 to $N_L$ and $V^*_{\mathrm{GPL}}$ is the total GPL volume fraction of the composite shell. The value of $V^*_{\mathrm{GPL}}$ can be determined by using the equation

$$V^*_{GPL} = \frac{W_{\mathrm{GPL}}}{W_{\mathrm{GPL}} + \left(\frac{\rho_{\mathrm{GPL}}}{\rho_m}\right)(1 - W_{\mathrm{GPL}})} \tag{2}$$

where $W_{\mathrm{GPL}}$, $\rho_{\mathrm{GPL}}$, and $\rho_m$ denote the mean weight fraction of GPLs, mass density of GPLs, and mass density of polymer matrix, respectively. As defined above, each layer is isotropic, and, as a result, the effective elastic modulus of the $k$-th layer is determined by the Halpin–Tsai micro-mechanical model [38] as

$$E^{(k)} = \frac{3}{8}\frac{1 + \xi_L \eta_L V^{(k)}_{\mathrm{GPL}}}{1 - \eta_L V^{(k)}_{\mathrm{GPL}}} \times E_{\mathrm{m}} + \frac{5}{8}\frac{1 + \xi_T \eta_T V^{(k)}_{\mathrm{GPL}}}{1 - \eta_T V^{(k)}_{\mathrm{GPL}}} \times E_m \tag{3}$$

where geometrical parameters $\xi_L$ and $\xi_T$ and auxiliary coefficients $\eta_L$ and $\eta_T$ are defined as follows

$$\xi_L = 2\left(\frac{a_{\mathrm{GPL}}}{t_{\mathrm{GPL}}}\right), \quad \xi_T = 2\left(\frac{b_{\mathrm{GPL}}}{t_{\mathrm{GPL}}}\right), \quad \eta_L = \frac{\left(\frac{E_{\mathrm{GPL}}}{E_m}\right) - 1}{\left(\frac{E_{\mathrm{GPL}}}{E_m}\right) + \xi_L}, \quad \eta_T = \frac{\left(\frac{E_{\mathrm{GPL}}}{E_m}\right) - 1}{\left(\frac{E_{\mathrm{GPL}}}{E_m}\right) + \xi_T} \tag{4}$$

in which $E_m$ and $E_{\mathrm{GPL}}$ are elastic moduli of the polymer matrix and GPLs. The average GPL thickness, width, and length are denoted by $t_{\mathrm{GPL}}$, $b_{\mathrm{GPL}}$, and $a_{\mathrm{GPL}}$, respectively. The effective Poisson's ratio and mass density of the $k$-th layer are predicted by the rule of mixture, as Poisson's ratio and mass density values of GPLs and polymer matrix are close to each other, and due to practical considerations, only small amounts of GPL are added to the matrix

$$\rho^{(k)} = \rho_{\mathrm{GPL}} V^{(k)}_{\mathrm{GPL}} + \rho_m V^{(k)}_m, \quad \nu^{(k)} = \nu_{\mathrm{GPL}} V^{(k)}_{\mathrm{GPL}} + \nu_m V^{(k)}_m \tag{5}$$

where subscripts "$m$" and "GPL" stand for matrix and GPLs, respectively.

## 3 Fundamental equations

In this article, the first-order shear deformation theory [39], which predicts the FG-GPLRC cylindrical shell's global displacement field by first-order terms and is suitable for thin to moderately thick shells, is employed

$$\begin{aligned} u_1(x_1, x_2, z, t) &= u(x_1, x_2, t) + z\,\psi_1(x_1, x_2, t) \\ u_2(x_1, x_2, z, t) &= v(x_1, x_2, t) + z\,\psi_2(x_1, x_2, t) \\ u_3(x_1, x_2, z, t) &= w(x_1, x_2, t) \end{aligned} \tag{6}$$

where $(u_1, u_2, u_3)$ and $(u, v, w)$ are the global and mid-plane displacements of the shell along longitudinal, circumferential, and radial directions, respectively. Middle surface rotations at $z = 0$ about $x_2$ and $x_1$ axes are denoted by $\psi_1$, $\psi_2$, respectively. According to Sanders' assumptions [40], the strain–displacement relationship can be expressed as

$$\begin{Bmatrix} \varepsilon_1 \\ \varepsilon_2 \\ \varepsilon_6 \end{Bmatrix} = \begin{Bmatrix} \varepsilon^0_1 \\ \varepsilon^0_2 \\ \varepsilon^0_6 \end{Bmatrix} + z \begin{Bmatrix} k_1 \\ k_2 \\ k_6 \end{Bmatrix}, \quad \varepsilon_4 = \frac{\partial w}{\partial x_2} + \psi_2 - \frac{v}{R}, \quad \varepsilon_5 = \frac{\partial w}{\partial x_1} + \psi_1 \tag{7}$$

where

$$\begin{aligned} \varepsilon^0_1 &= \tfrac{\partial u}{\partial x_1}, \quad \varepsilon^0_2 = \tfrac{\partial v}{\partial x_2} + \tfrac{w}{R}, \quad \varepsilon^0_6 = \tfrac{\partial v}{\partial x_1} + \tfrac{\partial u}{\partial x_2} \\ k_1 &= \tfrac{\partial \psi_1}{\partial x_1}, \quad k_2 = \tfrac{\partial \psi_2}{\partial x_2}, \quad k_6 = \tfrac{\partial \psi_2}{\partial x_1} + \tfrac{\partial \psi_1}{\partial x_2} \end{aligned} \tag{8}$$

The mathematical expressions for the stress components of each layer are obtained using constitutive relations based on the Hook law for linear elastic materials

$$\begin{Bmatrix}\sigma_1\\ \sigma_2\\ \sigma_6\end{Bmatrix}^{(k)}=\begin{bmatrix}Q_{11}^{(k)} & Q_{12}^{(k)} & 0\\ Q_{21}^{(k)} & Q_{22}^{(k)} & 0\\ 0 & 0 & Q_{66}^{(k)}\end{bmatrix}\begin{Bmatrix}\varepsilon_1\\ \varepsilon_2\\ \varepsilon_6\end{Bmatrix},\quad \begin{Bmatrix}\sigma_4\\ \sigma_5\end{Bmatrix}^{(k)}=\begin{bmatrix}Q_{44}^{(k)} & 0\\ 0 & Q_{55}^{(k)}\end{bmatrix}\begin{Bmatrix}\varepsilon_4\\ \varepsilon_5\end{Bmatrix} \tag{9}$$

in which $Q_{ij}^{(k)}$ are the elements of the material stiffness matrix, which can be calculated for each lamina as

$$Q_{11}^{(k)}=Q_{22}^{(k)}=\frac{E^{(k)}}{1-\nu^{(k)}\nu^{(k)}},\quad Q_{12}^{(k)}=Q_{21}^{(k)}=\frac{\nu^{(k)}E^{(k)}}{1-\nu^{(k)}\nu^{(k)}},\quad Q_{44}^{(k)}=Q_{55}^{(k)}=Q_{66}^{(k)}=\frac{E^{(k)}}{2\left(1+\nu^{(k)}\right)} \tag{10}$$

## 4 Governing partial differential equations

To obtain partial differential equations of vibrational motion, the Hamilton principle is employed [39]. The governing equations of the vibratory motion of the FG-GPLRC cylindrical shell in terms of stress resultants can be obtained as

$$\begin{aligned}
&\tfrac{\partial N_1}{\partial x_1}+\tfrac{\partial N_6}{\partial x_2}=I_1\ddot{u}+I_2\ddot{\psi}_1\\
&\tfrac{\partial N_6}{\partial x_1}+\tfrac{\partial N_2}{\partial x_2}+\tfrac{Q_2}{R}=I_1\ddot{v}+I_2\ddot{\psi}_2\\
&\tfrac{\partial M_1}{\partial x_1}+\tfrac{\partial M_6}{\partial x_2}-Q_1=I_2\ddot{u}+I_3\ddot{\psi}_1\\
&\tfrac{\partial M_6}{\partial x_1}+\tfrac{\partial M_2}{\partial x_2}-Q_2=I_2\ddot{v}+I_3\ddot{\psi}_2\\
&\tfrac{\partial Q_1}{\partial x_1}+\tfrac{\partial Q_2}{\partial x_2}-\tfrac{N_2}{R}=I_1\ddot{w}
\end{aligned} \tag{11}$$

The mathematical formulas for normal forces ($N_i$), shear forces ($Q_i$), and bending moments ($M_i$) can be defined as

$$\begin{Bmatrix}N_1\\ N_2\\ N_6\\ Q_1\\ Q_2\end{Bmatrix}=\sum_{k=1}^{N_L}\int_{z_{k-1}}^{z_k}\begin{Bmatrix}\sigma_1^{(k)}\left(1+\frac{z}{R}\right)\\ \sigma_2^{(k)}\\ \sigma_6^{(k)}\left(1+\frac{z}{R}\right)\\ k_s\sigma_5^{(k)}\left(1+\frac{z}{R}\right)\\ k_s\sigma_4^{(k)}\end{Bmatrix}\mathrm{d}z,\quad \begin{Bmatrix}M_1\\ M_2\\ M_6\end{Bmatrix}=\sum_{k=1}^{N_L}\int_{z_{k-1}}^{z_k}\begin{Bmatrix}\sigma_1^{(k)}\left(1+\frac{z}{R}\right)\\ \sigma_2^{(k)}\\ \sigma_6^{(k)}\left(1+\frac{z}{R}\right)\end{Bmatrix}z\,\mathrm{d}z \tag{12}$$

where $k_s$ is the shear correction factor. Additionally, $I_i$, where $i=1,2,3$ stands for mass inertia terms and can be written as

$$I_i=\sum_{k=1}^{N_L}\int_{z_{k-1}}^{z_k}\rho^{(k)}\left(1+\frac{z}{R}\right)z^{(i-1)}\mathrm{d}z,\quad (i=1,2,3) \tag{13}$$

Three classes of classical boundary conditions for the vibration of FG-GPLRC cylindrical shells, namely clamped (C), simply supported (S), and free (F) edges, are as follows

$$\begin{aligned}
&\mathrm{C}: w=\psi_1=\psi_2=u=v=0\\
&\mathrm{S}: w=M_1=\psi_2=u=v=0\\
&\mathrm{F}: N_1=N_6=M_1=M_6=Q_1=0
\end{aligned} \tag{14}$$

## 5 Solution method

The motion equations of the FG-GPLRC cylindrical shell in terms of stress resultants are composed of five partial differential equations. For the harmonic response of a cylindrical shell under Levy-type boundary conditions, the following displacement components are assumed, which enforce the periodic motion of the shell structure in free vibration

$$\begin{aligned} u &= U_m(x_1)\sin(\beta_m x_2)e^{i\omega_m t} \\ v &= V_m(x_1)\cos(\beta_m x_2)e^{i\omega_m t} \\ \psi_1 &= X_m(x_1)\sin(\beta_m x_2)e^{i\omega_m t} \\ \psi_2 &= Y_m(x_1)\cos(\beta_m x_2)e^{i\omega_m t} \\ w &= W_m(x_1)\sin(\beta_m x_2)e^{i\omega_m t} \end{aligned} \tag{15}$$

where $\beta_m$ is related to the circumferential mode number $m$ by $\beta_m = m\pi/R\theta$, $i$ is the imaginary unit ($i^2 = -1$), and the natural frequency of the $m$-th vibrating mode is denoted by $\omega_m$. Moreover, $U_m$, $V_m$, $X_m$, $Y_m$, and $W_m$ represent the mode shapes of the shell structure along the $x_1$ axis. To satisfy Levy requirements for boundary conditions of the cylindrical shell, we apply simply supported conditions at edges parallel to the $x_1$ axis. Edges at $x_1 = \pm L/2$ assume arbitrary boundary conditions. Substituting generalized displacement solutions in Eqs. (15) into (11) and after mathematical simplifications, equations of motion can be rewritten in the form of a system of five coupled linear ordinary differential equations (ODE) as follows

$$\begin{aligned} &p_1U + p_2U'' + p_3V' + p_4W' + p_5X + p_6X'' + p_7Y' = 0 \\ &p_8U' + p_9V + p_{10}V'' + p_{11}W + p_{12}X' + p_{13}Y + p_{14}Y'' = 0 \\ &p_{15}U + p_{16}U'' + p_{17}V' + p_{18}W' + p_{19}X + p_{20}X'' + p_{21}Y' = 0 \\ &p_{22}U' + p_{23}V + p_{24}V'' + p_{25}W + p_{26}X' + p_{27}Y + p_{28}Y'' = 0 \\ &p_{29}U' + p_{30}V + p_{31}W + p_{32}W'' + p_{33}X' + p_{34}Y = 0 \end{aligned} \tag{16}$$

In Eq. (16), differentiation with respect to $x_1$ is indicated by prime superscript, and $p_i$ coefficients are given in Appendix A. The five resulting second-order ODEs are solved using the state-space approach. Any $n$-th-order ODE can be transformed into $n$ first-order ODEs employing this technique. Similarly, five second-order ODEs, which govern the free vibration of the GPLRC cylindrical shell, are converted to ten first-order ODEs. To implement the strategy, the following ten state variables are taken into account

$$\begin{aligned} &Z_{1m}(x_1) = U_m(x_1), \quad Z_{2m}(x_1) = U_m'(x_1) = Z_{1m}'(x_1) \\ &Z_{3m}(x_1) = V_m(x_1), \quad Z_{4m}(x_1) = V_m'(x_1) = Z_{3m}'(x_1) \\ &Z_{5m}(x_1) = W_m(x_1), \quad Z_{6m}(x_1) = W_m'(x_1) = Z_{5m}'(x_1) \\ &Z_{7m}(x_1) = X_m(x_1), \quad Z_{8m}(x_1) = X_m'(x_1) = Z_{7m}'(x_1) \\ &Z_{9m}(x_1) = Y_m(x_1), \quad Z_{10m}(x_1) = Y_m'(x_1) = Z_{9m}'(x_1) \end{aligned} \tag{17}$$

After applying the change of variables and defining $\{Z\}$ and $\{Z'\}$ vectors as $\{Z\} = \{Z_{1m} \quad Z_{2m} \quad \dots \quad Z_{10m}\}^T$ and $\{Z'\} = \{Z'_{1m} \quad Z'_{2m} \quad \dots \quad Z'_{10m}\}^T$, the ordinary differential equations of motion are finally recast as a set of equations that can be aggregated in the matrix form as

$$\{Z'\} = [A]\{Z\} \tag{18}$$

where $[A]$ is a $10 \times 10$ square matrix. The solution to this set of equations assumes the following form [39,41]

$$\{Z(x_1)\} = e^{[A]x_1}\{K\} \tag{19}$$

where $\{K\}$ is a vector containing the information about the boundary conditions that were applied to the shell structure. The exponential form of the $[A]$ matrix can be determined by the modal matrix approach, which reads

$$e^{[A]x_1} = [M]\begin{bmatrix} e^{\lambda_1 x_1} & & & 0 \\ & e^{\lambda_2 x_1} & & \\ & & \ddots & \\ 0 & & & e^{\lambda_{10} x_1} \end{bmatrix}[M]^{-1} \tag{20}$$

**Table 1** Mechanical properties of the GPL reinforcements and epoxy matrix

| Properties | GPL | Epoxy |
|---|---|---|
| Young's modulus ($E$) GPa | 1010 | 3.0 |
| Mass density ($\rho$) kg/m$^3$ | 1060 | 1200 |
| Poisson's ratio ($\nu$) | 0.186 | 0.34 |

**Table 2** Dimensionless natural frequencies of SSSS FG-GPLRC cylindrical shells with various $L/h$ ratios for $R/L = 5$, $L = b = 0.45$ m, $N_L = 12$, and $W_{\mathrm{GPL}} = 1\%$

| $(m, n)$ | $L/h$ | Pattern | Present | Ref. [34] |
|---|---|---|---|---|
| (1, 1) | 10 | Pattern 1 | 0.12291 | 0.12293 |
| | | Pattern 2 | 0.10290 | 0.10402 |
| | | Pattern 3 | 0.13952 | 0.13762 |
| | 20 | Pattern 1 | 0.03281 | 0.03281 |
| | | Pattern 2 | 0.02774 | 0.02797 |
| | | Pattern 3 | 0.03714 | 0.03689 |
| | 50 | Pattern 1 | 0.00652 | 0.00652 |
| | | Pattern 2 | 0.00587 | 0.00589 |
| | | Pattern 3 | 0.00711 | 0.00708 |
| (2, 1) | 10 | Pattern 1 | 0.28923 | 0.28923 |
| | | Pattern 2 | 0.24331 | 0.24669 |
| | | Pattern 3 | 0.32590 | 0.31794 |
| | 20 | Pattern 1 | 0.07700 | 0.07700 |
| | | Pattern 2 | 0.06389 | 0.06457 |
| | | Pattern 3 | 0.08793 | 0.08697 |
| | 50 | Pattern 1 | 0.01265 | 0.01265 |
| | | Pattern 2 | 0.01049 | 0.01058 |
| | | Pattern 3 | 0.01449 | 0.01440 |
| (2, 2) | 10 | Pattern 1 | 0.44366 | 0.44377 |
| | | Pattern 2 | 0.37553 | 0.38282 |
| | | Pattern 3 | 0.49570 | 0.47982 |
| | 20 | Pattern 1 | 0.12191 | 0.12192 |
| | | Pattern 2 | 0.10158 | 0.10272 |
| | | Pattern 3 | 0.13859 | 0.13679 |
| | 50 | Pattern 1 | 0.02046 | 0.02046 |
| | | Pattern 2 | 0.01706 | 0.01721 |
| | | Pattern 3 | 0.02335 | 0.02320 |

in which $[M]$ is the eigenvectors of the square matrix $[A]$ and $\lambda_i$ (i=1, 2, …, 10) are the eigenvalues of the square matrix $[A]$. Considering different configurations of the boundary conditions at the edges $x_1 = \pm L/2$ and incorporating the associated details in Eq. (19), a homogeneous system of equations is found as

$$[G]\{K\} = 0 \tag{21}$$

where $[G]$ is the coefficient matrix. By setting the determinant of the coefficient matrix to zero, the characteristic equation is obtained. Solving for the roots of the characteristic equation provides the natural frequencies of the FG-GPLRC cylindrical shell.

## 6 Results and discussions

An analysis method for the free vibrations of FG-GPLRC cylindrical shells was established in the earlier sections. First, comparative studies are carried out in this part. The precision and efficiency of the methods used to analyze the cylindrical shell behavior are then demonstrated using novel numerical data. In our paper, the computation time for a typical single computation was reported as 1.0413 s on an M3 processor with an 8-core CPU, 8.0GB of installed RAM, and a macOS operating system, with the frequency accuracy measured to 3 decimal places in Hertz units. Unless stated otherwise, a shell structure with GPLs serving as fillers and epoxy serving as the matrix is examined. Table 1 contains a list of the material characteristics of these components. For various geometrical parameters and material properties, parametric studies are carried out in

**Table 3** Comparison of fundamental natural frequencies of SSSS and SCSC CNTRC square plates with various $a/h$ ratios against experimental and FEM results from [43] for $W_{\mathrm{CNT}} = 0.1\%$

| Boundary condition | $a/h$ | Experiment [43] | FEM [43] | Present |
|---|---|---|---|---|
| SSSS | 100 | 60 | 63.267 | 62.947 |
| | 80 | 80 | 80.696 | 78.668 |
| | 60 | 104 | 107.43 | 104.84 |
| | 40 | 156 | 157.85 | 157.07 |
| SCSC | 100 | 92 | 93.636 | 92.270 |
| | 80 | 120 | 119.24 | 115.28 |
| | 60 | 160 | 158.56 | 153.53 |
| | 40 | 230 | 232.75 | 229.57 |

**Table 4** Natural frequencies (Hz) of FG-GPLRC cylindrical shells with various boundary conditions for different FG patterns and mode numbers ($L/h = 10$, $L/R = 1$, $R = 1$ m, $\theta = 90°$, $N_L = 12$, and $W_{\mathrm{GPL}} = 1\%$)

| BCs | Pattern | Mode number $(m, n)$ | | | |
|---|---|---|---|---|---|
| | | (1, 1) | (1, 2) | (2, 1) | (2, 2) |
| SCSC | U | 499.9 | 993.4 | 523.1 | 1053.2 |
| | O | 457.9 | 865.1 | 445.6 | 899.8 |
| | X | 535.0 | 1088.7 | 584.0 | 1165.0 |
| SCSS | U | 446.0 | 885.0 | 463.7 | 955.1 |
| | O | 418.0 | 772.9 | 394.7 | 813.2 |
| | X | 470.6 | 963.1 | 519.1 | 1061.7 |
| SSSS | U | 406.7 | 640.5 | 417.4 | 870.6 |
| | O | 389.2 | 640.7 | 354.3 | 738.3 |
| | X | 423.1 | 640.7 | 469.4 | 974.5 |
| SCSF | U | 212.5 | 570.9 | 273.7 | 606.4 |
| | O | 204.5 | 525.7 | 224.9 | 517.8 |
| | X | 219.6 | 609.6 | 313.2 | 676.7 |
| SSSF | U | 60.0 | 503.7 | 249.0 | 551.7 |
| | O | 47.8 | 475.4 | 199.3 | 471.6 |
| | X | 70.0 | 526.6 | 288.9 | 617.0 |
| SFSF | U | 41.6 | 81.7 | 221.4 | 306.8 |
| | O | 33.1 | 65.6 | 177.1 | 246.5 |
| | X | 48.5 | 94.5 | 257.1 | 354.6 |

order to assess the influences on the vibrational behavior of the associated structures under various boundary conditions. Letter symbols are used to describe the boundary conditions. For example, a panel with edges simply supported (S) at $x_2 = 0$, clamped (C) at $x_1 = -L/2$, simply supported (S) at $x_2 = R\theta$, and free (F) at $x_1 = L/2$ is represented by SCSF abbreviation. The $m$ and $n$ letters in the $(m, n)$ symbol indicate the associated vibrating mode's number of half-waves in the circumferential and axial directions, respectively. Graphs are presented to display numerical outcomes.

## 6.1 Validation of results

Unless otherwise stated, a stratification number of $N_L = 12$ is employed throughout this study [34]. Moreover, length, width, and thickness of the nanoplatelets [34] are set to be $a_{\mathrm{GPL}} = 2.5$ μm, $b_{\mathrm{GPL}} = 1.5$ μm, and $t_{\mathrm{GPL}} = 1.5$ nm, respectively. In using FSDT, shear correction factors are incorporated to address discrepancies between true transverse shear force distributions and those calculated through the kinematic relations of the FSDT, modifying the shell transverse shear stiffnesses to ensure that the strain energy due to transverse shear stresses equals the strain energy due to true transverse stresses predicted by three-dimensional elasticity theory [42]. Since transverse shear strains are modeled to be uniformly distributed through the shell thickness, transverse shear stresses are consequently constant. To rectify the disparity between the actual stress state and the constant stress state predicted by the first-order shear deformation theory, a correction is applied solely in the energy sense by introducing the shear correction factor. The actual value of the shear correction factor is dependent on the geometry and material properties of the shell. The impact of the shear correction factor is evident in frequency reduction; specifically, smaller shear correction factors correspond to smaller frequencies.

However, within acceptable and realistic ranges, the variation in shear correction factor has minimal influence on the natural frequencies of structures. Consequently, a shear correction of $5/6$ is widely adopted in numerous engineering applications without compromising calculation accuracy [39]. As mentioned before in the literature survey and to the best of the authors' knowledge, no article considers an analytical solution based on the state-space Levy approach for the natural frequencies of FG-GPLRC cylindrical shells under various boundary conditions. Therefore, a comparison study is conducted in Table 2 between the present results and those obtained by Wang et al. [34] on the non-dimensional frequencies of simply supported FG-GPLRC cylindrical shallow shells. The natural frequencies are reported for different mode numbers and three different patterns adopted in the above-mentioned research. A good agreement is achieved between the present results and those reported in the mentioned article on the dimensionless natural frequencies of the simply supported shell with different $L/h$ ratios. In another comparison study in Table 3, fundamental natural frequencies of SSSS and SCSC CNTRC square plates with various $a/h$ ratios are tabulated against experimental and finite element method (FEM) results provided by Patel et al. [43]. The accuracy of the proposed method is proved by the good agreement between the present results and the experimental/FEM results of the reference work.

### 6.2 Parametric studies

The natural frequencies of FG-GPLRC cylindrical shells with various boundary conditions are tabulated in Table 4 for different FG patterns and mode numbers. Stiffer support types make a positive contribution to the general rigidity of the structure, and higher natural frequencies are obtained for more rigid boundary conditions. A general trend is observed for the same edge configurations and the same mode numbers, as FG-X and FG-O composites possess the highest and lowest stiffness among the dispersion patterns, respectively.

For three different GPL distribution patterns along the thickness of a composite shell that is simply supported at all edges (SSSS), the first and second natural frequencies are plotted in Fig. 2 versus the total weight fraction of GPLs. The results show that the addition of GPLs noticeably enhances both the first and second natural frequencies of the shell structure. As expected, higher GPL content results in better enhancement of the shell stiffness and increases the fundamental and second natural frequencies of the system. Moreover, among the distribution patterns and for the same amount of GPL weight fraction, FG-X composite shells exhibit the highest first and second frequencies, whereas the lowest frequency values are obtained for shells made of FG-O composite. This trend implies that more GPL fillers in the top and bottom layers of the shell considerably improve the elastic stiffness and accordingly contribute to the mechanical behavior of the structure.

For cylindrical composite shells that are simply supported at all edges (SSSS) with three different GPL distribution patterns along the thickness direction, the first and second natural frequencies are presented in Fig. 3 versus the stratification number. Notably, when the stratification number exceeds 15, both frequencies remain relatively stable across all patterns. Not surprisingly, due to the homogeneous distribution of GPL fillers in the FG-U pattern, the first two frequencies of FG-GPLRC shells remain constant despite varying stratification numbers. Conversely, the frequencies of FG-O and FG-X composite shells are considerably affected by stratification number. The FG-O pattern exhibits a decrease in both frequencies as the stratification number increases; however, the FG-X pattern demonstrates the opposite behavior. Knowing that the mean GPL weight fraction is constant, by increasing the number of layers for the FG-X pattern, the high-stiffness layers with higher reinforcements are pushed toward the top and bottom surfaces of the shell structure, and this causes a higher stiffness compared to the FG-U pattern. Conversely, for the FG-O pattern, increasing the number of layers will concentrate most of the nanofillers close to the center of the composite shell, which in turn will result in lower overall stiffness.

Figure 4 depicts the variation in the first two natural frequencies of SSSS FG-GPLRC cylindrical shells with three different GPL distribution patterns against shallowness angle $\theta$. It is generally observed that the frequencies exhibit a decreasing trend with increasing shallowness angles, owing to the reduction in the rigidity of the structure. As shown in Fig. 4a, the alterations in the shallowness angle serve as a cause for the switching mode phenomenon in fundamental frequency, as an increase in the shallowness angle results in the reduction in the panel's flexural rigidity, consequently leading to higher half-waves in the circumferential direction. For FG-O composite shells, the mode switching from $m = 1$ to $m = 2$ occurs at about $\theta = 97°$, whereas for FG-U and FG-X composites, it appears at higher values of $\theta$ compared to FG-O shells as their flexural rigidity is generally higher than their FG-O counterparts. As depicted in Fig. 4b, the mode switching is also observable in the second natural frequency of the shell structure. The first mode shift from $m = 1$ to $m = 2$ arises at about $\theta = 69°$ for FG-O composites, and the second mode change is observed again at $\theta = 97°$, where the

mode switching for fundamental frequency happens. Similar to the observations for fundamental frequency, in second frequency, mode switching for FG-U and FG-X composites is at higher values of $\theta$.

The effect of sallowness angle on the first two natural frequencies of FG-GPLRC cylindrical shells under various boundary conditions is investigated in Fig. 5. Results are graphically represented for all six possible boundary combinations of the Levy- type, namely SCSC, SCSS, SSSS, SCSF, SSSF, and SFSF. A general downward trend in frequencies for increasing values of $\theta$ is confirmed for all sets of boundary conditions, which is similar to our finding in Fig. 4. Support types with higher rigidity, namely SCSC, SCSS, and SSSS, behave similarly in terms of both the variation in frequencies and mode switching. As it can be seen in Fig. 5a, the mode shift in fundamental frequency of SCSC, SCSS, and SSSS shells emerges at shallowness angles of $\theta = 95°, 96°$, and $97°$, whereas no switching in fundamental frequency is detected for SCSF, SSSF, and SFSF composites. As shown in Fig. 5b, for the second natural frequency of the panels with no free edges, first and second mode shifts take place at approximate shallowness angles of $\theta = 67°, 68°, 69°$ and $\theta = 95°, 96°, 97°$, respectively. The only detectable mode shifts in second frequencies of the structures with a single free edge, namely SCSF and SSSF shells, are at about $\theta = 79°$ and $\theta = 80°$, respectively. Moreover, no switching is observed for SFSF shells.

Figure 6a, b shows the effect of changing the length-to-radius ratio on the first two frequencies of FG-O composite cylindrical shells under various boundary conditions. It can be posited that increasing the length-to-radius ratio $L/R$ results in a decline in the natural frequencies of the cylindrical shells under different sets of boundary conditions. This observation can be attributed to the reduction in the bending stiffness of the panel when the $L/R$ ratio is larger. One can easily discern that the $L/R$ ratio has a marginal impact on the first two frequencies of SSSF and SFSF cylindrical shells. This behavior occurs since the length ratio of the shell structure plays a crucial role in determining the stiffness and mass distribution across the laminated shell. As the length ratio increases, the shell's stiffness becomes more noticeable in the shorter direction (edges are simply supported due to the Levy requirement along this direction) compared to the longer one, thereby influencing the natural frequencies. With a growing aspect ratio, the shell structure becomes more flexible along its length, leading to a reduction in stiffness and, consequently, natural frequencies. The presence of free edges allows for greater motion. As a result, an increase in the number of free edges in the structure reduces the impact of the length ratio on the natural frequencies. This suggests that the geometric (essential) boundary conditions exert a more substantial influence on the vibration of the composite cylindrical shell than the natural boundary conditions. Furthermore, mode switching occurs for SCSF composites at about $L/R = 1.43$.

The lowest natural frequencies of SSSS and SCSC FG-O composite cylindrical shells associated with different shell thicknesses and mode numbers are provided in Fig. 7. Based on the data presented, by altering the total thickness of the shell, the circumferential half-wave number of the fundamental frequency undergoes a change. When the thicknesses of SSSS and SCSC cylindrical shells are 2 cm and 3 cm, the circumferential mode number corresponding to fundamental frequencies is $m = 3$. For other thicknesses presented in the figure, the fundamental frequencies are associated with the circumferential mode number $m = 2$. It is important to note that a slight change can be observed in the frequency of the mode associated with $m = 1$ by increasing the panel thickness for both SSSS and SCSC shells. However, for other circumferential mode numbers, a positive correlation prevails between the thickness of the panel and the related natural frequency. The modes of vibration involved determine how natural frequencies behave in shells with rigid boundary constraints. Vibration in the first mode, often known as the fundamental mode, typically results in a more global structural deformation. When the boundary conditions are quite rigid, the first mode's frequency remains essentially stable for the thickness values provided in this figure, due to the strict boundary requirements that help limit the total response. On the other hand, there is a complicated interaction between mass distribution and bending stiffness for higher modes. Consequently, the deformation behavior becomes increasingly complicated and localized at higher modes of vibration. The global response is still governed by rigid boundary constraints, but higher modes are more sensitive to variations in structural parameters like thickness due to their increased level of complexity. Also, it is noteworthy that a narrow range of thickness variation is considered here.

## 7 Conclusions

In this article, exact solutions based on the state-space Levy approach for free vibrations of FG-GPLRC cylindrical shells under various boundary conditions are presented. In-plane global displacements are assumed to be linear functions of the coordinate along the thickness of the shell, according to the first-order shear deformation theory. The assumptions of Sanders are adopted for strain–displacement relations. The effect of

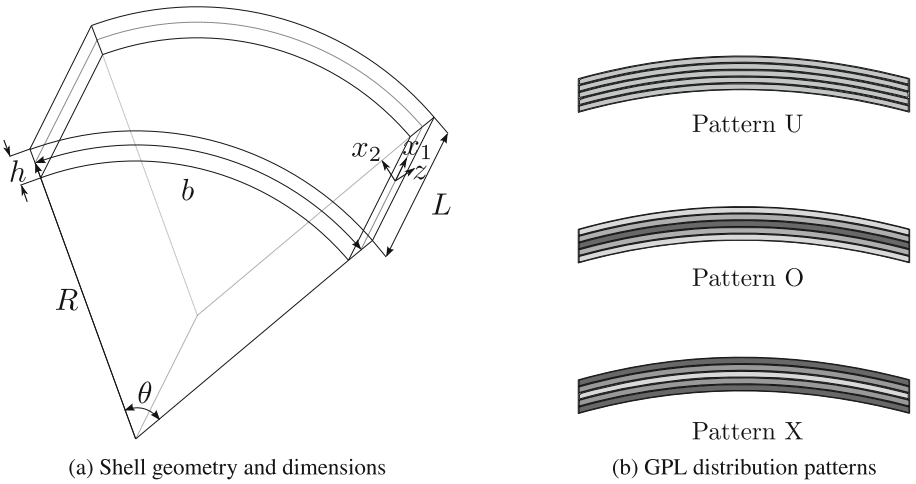


(a) Shell geometry and dimensions

(b) GPL distribution patterns

**Fig. 1** Schematic of a GPLRC cylindrical shell

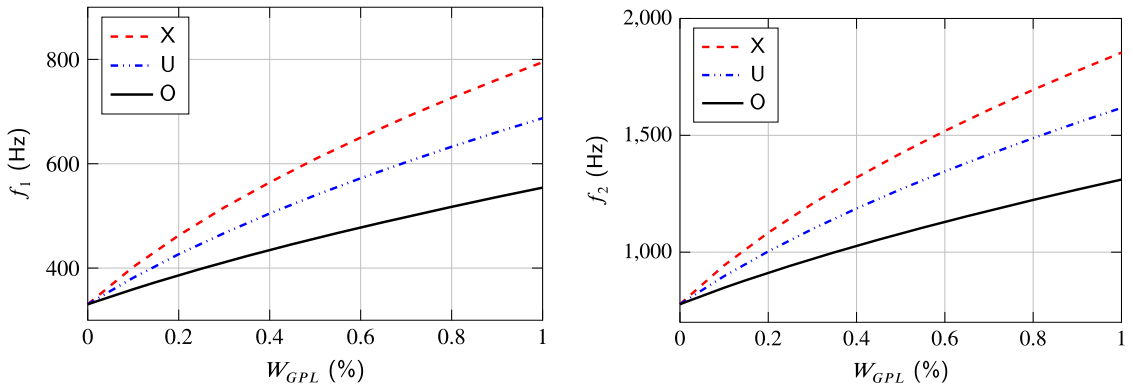


(a) First natural frequency

(b) Second natural frequency

**Fig. 2** First two frequencies of SSSS FG-GPLRC cylindrical shells with three distribution patterns versus GPL weight fraction for $L/h = 10$, $L/R = 0.2$, $L = b = 0.45$ m, and $N_L = 12$: **a** first natural frequency; **b** second natural frequency

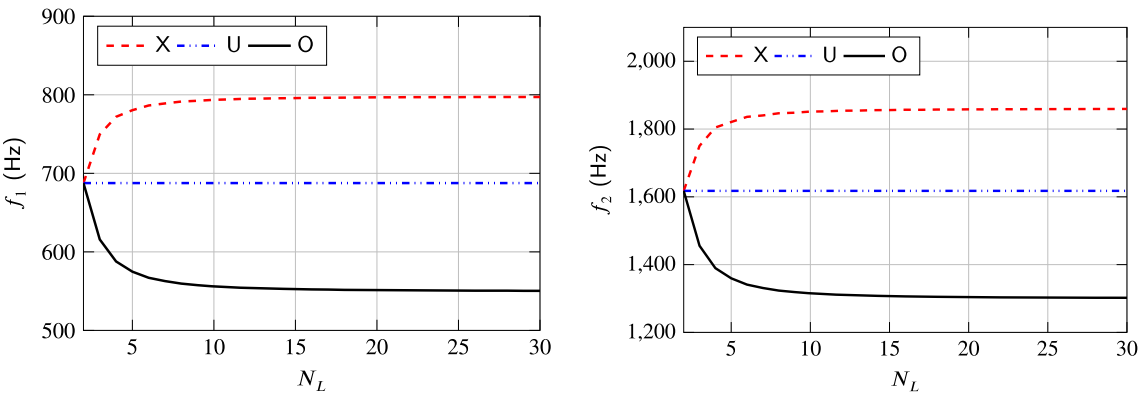


(a) First natural frequency

(b) Second natural frequency

**Fig. 3** First two frequencies of SSSS FG-GPLRC cylindrical shells with three distribution patterns versus stratification number for $L/h = 10$, $L/R = 0.2$, $L = b = 0.45$ m, and $W_{\mathrm{GPL}} = 1\%$: **a** first natural frequency; **b** second natural frequency

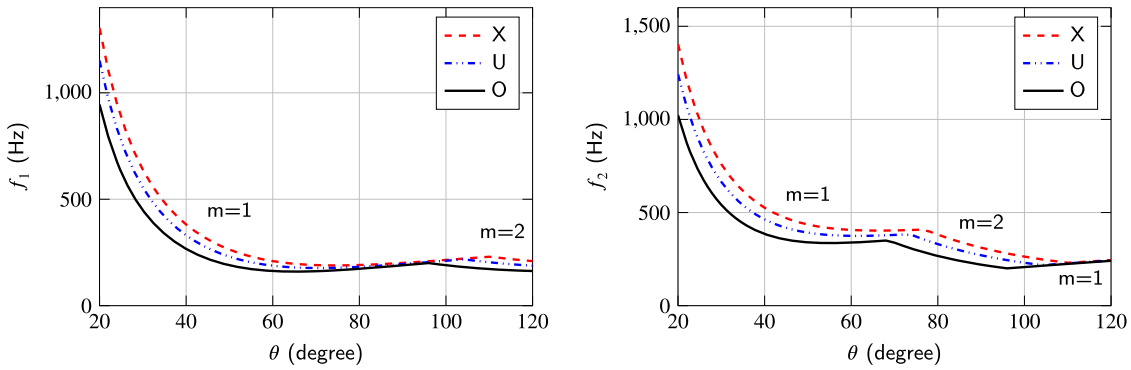


(a) First natural frequency (b) Second natural frequency

**Fig. 4** First two frequencies of SSSS FG-GPLRC cylindrical shells with three distribution patterns versus shallowness angle for $h/R = 0.1$, $L/R = 2$, $R = 1$ m, $N_L = 12$, and $W_{\mathrm{GPL}} = 1\%$: **a** first natural frequency; **b** second natural frequency

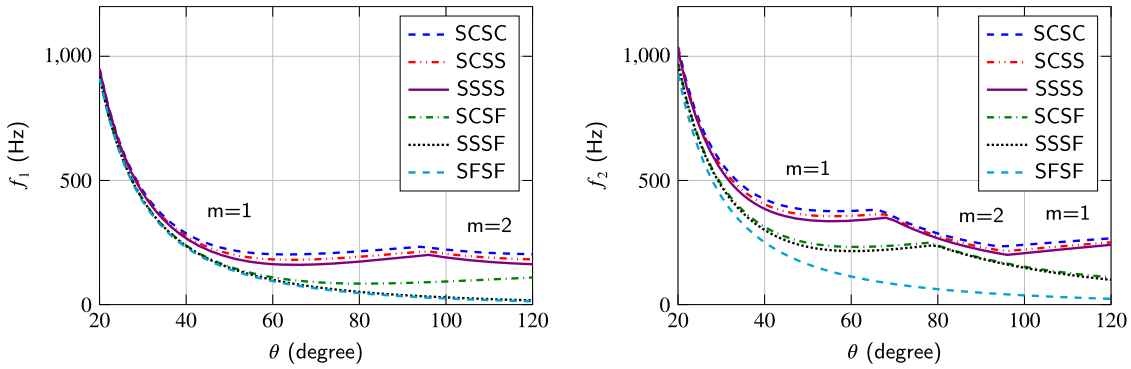


(a) First natural frequency (b) Second natural frequency

**Fig. 5** First two frequencies of FG-O composite cylindrical shells under various boundary conditions versus shallowness angle for $h/R = 0.1$, $L/R = 2$, $R = 1$ m, $N_L = 12$, and $W_{\mathrm{GPL}} = 1\%$: **a** first natural frequency; **b** second natural frequency

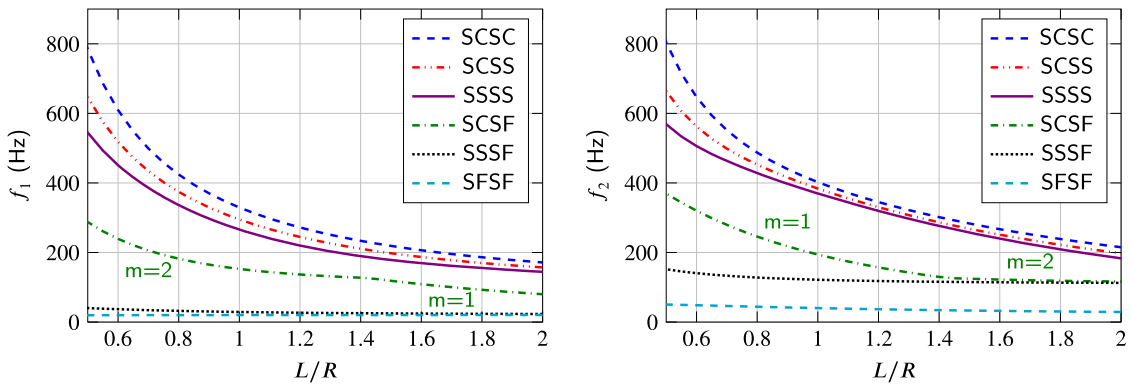


(a) First natural frequency (b) Second natural frequency

**Fig. 6** First two frequencies of FG-O composite cylindrical shells under various boundary conditions versus length-to-radius ratio for $h/R = 0.06$, $\theta = 90°$, $R = 1$ m, $N_L = 12$, and $W_{\mathrm{GPL}} = 1\%$: **a** first natural frequency; **b** second natural frequency

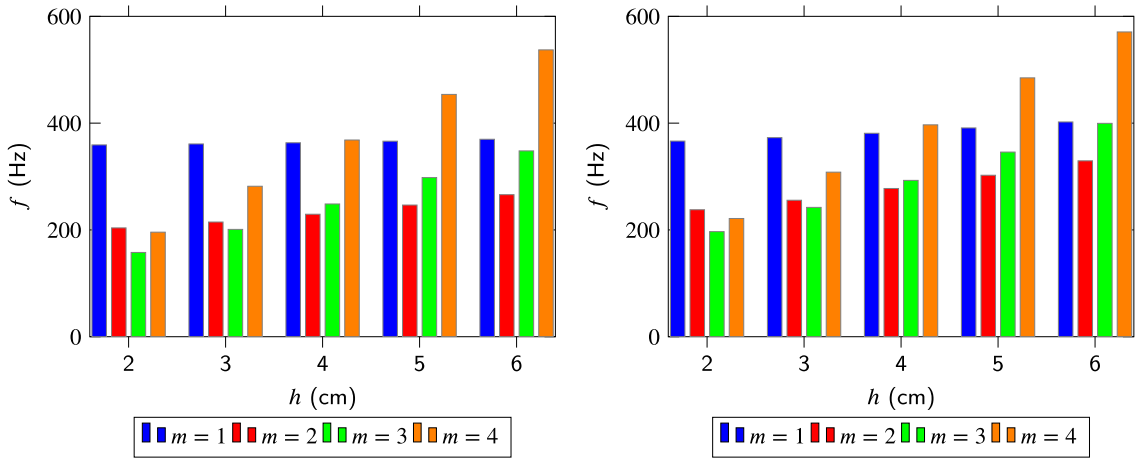


(a) SSSS FG-GPLRC shells

(b) SCSC FG-GPLRC shells

**Fig. 7** Natural frequencies of FG-O composite cylindrical shells with different shell thicknesses and mode numbers for $L/R = 1$, $\theta = 90°$, $R = 1$ m, $N_L = 12$, and $W_{\text{GPL}} = 1\%$: **a** SSSS FG-GPLRC shells; **b** SCSC FG-GPLRC shells

GPL weight fraction, stratification number, GPL distribution pattern, shallowness angle, and other geometrical parameters, namely thickness and length-to-radius ratio, on the natural frequencies of the panel is examined using a series of parametric studies, and the free vibration frequencies are reported for different mode numbers and boundary conditions. This study also yields the following conclusions:

- The circumferential mode number associated with the fundamental frequency of the FG-GPLRC shell is sensitive to variations in support types, shallowness angle, and geometrical ratios.
- Mode switching is affected by variations in boundary conditions, shallowness angle, and length ratios. To elaborate further, mode switching takes place at different length ratios and shallowness angles depending on the rigidity of the boundary conditions. In stiffer configurations such as SCSC, SCSS, and SSSS, mode switching in the second frequencies occurs at lower values of shallowness angles ($\theta \approx 68°$) compared to less stiff setups ($\theta \approx 96°$). Additionally, the variation in length ratio and shallowness angle plays a pivotal role in determining the stiffness and mass distribution across the laminated shell. With an increase in the length ratio, the shell's stiffness becomes more evident in the circumferential direction, while an increase in the shallowness angle accentuates the longitudinal stiffness.
- As expected, the rigidity of different boundary configurations affects the natural frequencies of the FG-GPLRC cylindrical shell. For the configuration in Fig. 5 and $\theta = 90°$, the fundamental frequency of SCSC shells is approximately 7 times the frequency of SFSF shells.
- GPL-reinforced cylindrical shells with layers stacked up according to the FG-X pattern exhibit the highest stiffness and frequencies among the examined patterns (depending on the shell configurations, approximately 45 percent higher compared to the FG-O pattern for simply supported shells).
- A considerably small amount (0.2 percent weight fraction) of GPL reinforcement gives rise to an almost 50 percent enhancement of the frequencies of the simply supported shells.
- A layered GPLRC shell structure with stratification numbers of $N_L = 10$ or higher provides an appropriate functionally graded composition for stiffness improvement in the structure.

The findings of this study can serve as a fundamental benchmark solution for forthcoming research pertaining to the free vibration of FG-GPLRC shells. It is crucial to consider the associations between the frequencies and geometrical parameters, boundary conditions, and mode numbers for the sake of future applications.

**Funding** Open access funding provided by TU Wien (TUW). Open access funding provided by TU Wien Bibliothek (TUW).

**Declarations**

**Conflict of interest** The authors have no relevant financial or non-financial interests to disclose.

## A Appendix

$$p_1 = I_1\omega^2 - \beta^2\left(A_{66} + \frac{B_{66}}{R}\right), \quad p_2 = A_{11} + \frac{B_{11}}{R}, \quad p_3 = -\beta\left(A_{12} + \frac{B_{12}}{R} + A_{66} + \frac{B_{66}}{R}\right) \tag{22a}$$

$$p_4 = \frac{1}{R}\left(A_{12} + \frac{B_{12}}{R}\right), \quad p_5 = I_2\omega^2 - \beta^2\left(B_{66} + \frac{C_{66}}{R}\right), \quad p_6 = B_{11} + \frac{C_{11}}{R} \tag{22b}$$

$$p_7 = -\beta\left(B_{12} + \frac{C_{12}}{R} + B_{66} + \frac{C_{66}}{R}\right), \quad p_8 = \beta\left(A_{21} + A_{66} + \frac{B_{66}}{R}\right) \tag{22c}$$

$$p_9 = I_1\omega^2 - A_{22}\beta^2 - k_s\frac{A_{44}}{R^2}, \quad p_{10} = A_{66} + \frac{B_{66}}{R}, \quad p_{11} = \beta\left(\frac{A_{22}}{R} + k_s\frac{A_{44}}{R}\right) \tag{22d}$$

$$p_{12} = \beta\left(B_{21} + B_{66} + \frac{C_{66}}{R}\right), \quad p_{13} = I_2\omega^2 - B_{22}\beta^2 + k_s\frac{A_{44}}{R}, \quad p_{14} = B_{66} + \frac{C_{66}}{R} \tag{22e}$$

$$p_{15} = I_2\omega^2 - \beta^2\left(B_{66} + \frac{C_{66}}{R}\right), \quad p_{16} = B_{11} + \frac{C_{11}}{R}, \quad p_{17} = -\beta\left(B_{12} + \frac{C_{12}}{R} + B_{66} + \frac{C_{66}}{R}\right) \tag{22f}$$

$$p_{18} = \frac{1}{R}\left(B_{12} + \frac{C_{12}}{R}\right) - k_s\left(A_{55} + \frac{B_{55}}{R}\right), \quad p_{19} = I_3\omega^2 - k_s\left(A_{55} + \frac{B_{55}}{R}\right) - \beta^2\left(C_{66} + \frac{D_{66}}{R}\right) \tag{22g}$$

$$p_{20} = C_{11} + \frac{D_{11}}{R}, \quad p_{21} = -\beta\left(C_{12} + \frac{D_{12}}{R} + C_{66} + \frac{D_{66}}{R}\right), \quad p_{22} = \beta\left(B_{21} + B_{66} + \frac{C_{66}}{R}\right) \tag{22h}$$

$$p_{23} = I_2\omega^2 - B_{22}\beta^2 + k_s\frac{A_{44}}{R}, \quad p_{24} = B_{66} + \frac{C_{66}}{R}, \quad p_{25} = \beta\left(-k_sA_{44} + \frac{B_{22}}{R}\right) \tag{22i}$$

$$p_{26} = \beta\left(C_{21} + C_{66} + \frac{D_{66}}{R}\right), \quad p_{27} = I_3\omega^2 - k_sA_{44} - C_{22}\beta^2, \quad p_{28} = C_{66} + \frac{D_{66}}{R} \tag{22j}$$

$$p_{29} = -\frac{A_{21}}{R}, \quad p_{30} = \beta\left(\frac{A_{22}}{R} + k_s\frac{A_{44}}{R}\right), \quad p_{31} = I_1\omega^2 - k_sA_{44}\beta^2 - \frac{A_{22}}{R^2} \tag{22k}$$

$$p_{32} = k_s\left(A_{55} + \frac{B_{55}}{R}\right), \quad p_{33} = k_s\left(A_{55} + \frac{B_{55}}{R}\right) - \frac{B_{21}}{R}, \quad p_{34} = \beta\left(-k_sA_{44} + \frac{B_{22}}{R}\right) \tag{22l}$$

Unknown coefficients are:

$$[A_{11}, B_{11}, C_{11}, D_{11}] = \sum_{k=1}^{N_L}\int z^i\, Q_{11}^{(k)}\mathrm{d}z \quad (i = 0, 1, 2, 3) \tag{23a}$$

$$[A_{12}, B_{12}, C_{12}, D_{12}] = \sum_{k=1}^{N_L}\int z^i\, Q_{12}^{(k)}\mathrm{d}z \quad (i = 0, 1, 2, 3) \tag{23b}$$

$$[A_{21}, B_{21}, C_{21}, D_{21}] = \sum_{k=1}^{N_L}\int z^i\, Q_{21}^{(k)}\mathrm{d}z \quad (i = 0, 1, 2, 3) \tag{23c}$$

$$[A_{22}, B_{22}, C_{22}, D_{22}] = \sum_{k=1}^{N_L}\int z^i\, Q_{22}^{(k)}\mathrm{d}z \quad (i = 0, 1, 2, 3) \tag{23d}$$

$$[A_{66}, B_{66}, C_{66}, D_{66}] = \sum_{k=1}^{N_L} \int z^i \, Q_{66}^{(k)} \mathrm{d}z \quad (i = 0, 1, 2, 3) \tag{23e}$$

$$[A_{44}, B_{44}] = \sum_{k=1}^{N_L} \int z^i \, Q_{44}^{(k)} \mathrm{d}z \quad (i = 0, 1) \tag{23f}$$

$$[A_{55}, B_{55}] = \sum_{k=1}^{N_L} \int z^i \, Q_{55}^{(k)} \mathrm{d}z \quad (i = 0, 1) \tag{23g}$$

## References


1. Barthwal, S., Barthwal, S., Singh, N.: Nanocomposites and their sensing properties. (2022)
2. Bhattacharya, S.N., Gupta, R.K., Kamal, M.R.: Polymeric Nanocomposites. Hanser, Munich (2008)
3. Kausar, A.: Graphene to Polymer/Graphene Nanocomposites: Emerging Research and Opportunities. Elsevier, Amsterdam (2021)
4. Kitipornchai, S., Chen, D., Yang, J.: Free vibration and elastic buckling of functionally graded porous beams reinforced by graphene platelets. Mater. Des. **116**, 656–665 (2017)
5. Jafari, P., Kiani, Y.: A four-variable shear and normal deformable quasi-3d beam model to analyze the free and forced vibrations of FG-GPLRC beams under moving load. Acta Mech. **233**, 2797–2814 (2022)
6. Feng, C., Kitipornchai, S., Yang, J.: Nonlinear free vibration of functionally graded polymer composite beams reinforced with graphene nanoplatelets (GPLs). Eng. Struct. **140**, 110–119 (2017)
7. Bahranifard, F., Golbahar Haghighi, M., Malekzadeh, P.: In-plane responses of multilayer FG-GPLRC curved beams in thermal environment under moving load. Acta Mech. **231**, 2679–2696 (2020)
8. Zhang, L., Xu, Z., Gao, M., Xu, R., Wang, G.: Static, dynamic and buckling responses of random functionally graded beams reinforced by graphene platelets. Eng. Struct. **291**, 116476 (2023)
9. Zhang, X., Chen, B., Shao, Z., Wang, Q., Xiang, P.: A novel stochastic calculation scheme for dynamic response analysis of FG-GPLRC plate subject to a moving load. Acta Mech. **235**(4), 1803–1822 (2023)
10. Zhao, Z., Feng, C., Wang, Y., Yang, J.: Bending and vibration analysis of functionally graded trapezoidal nanocomposite plates reinforced with graphene nanoplatelets (GPLs). Compos. Struct. **180**, 799–808 (2017)
11. Yang, Y., Li, J.-A., Chen, B., Dong, Y., Li, Y.: Symmetric and asymmetric vibrations of rotating GPLRC annular plate. Int. J. Mech. Sci. **250**, 108282 (2023)
12. Sahmani, S., Aghdam, M.M., Rabczuk, T.: Nonlocal strain gradient plate model for nonlinear large-amplitude vibrations of functionally graded porous micro/nano-plates reinforced with GPLs. Compos. Struct. **198**, 51–62 (2018)
13. Karami, B., Shahsavari, D., Janghorban, M., Tounsi, A.: Resonance behavior of functionally graded polymer composite nanoplates reinforced with graphene nanoplatelets. Int. J. Mech. Sci. **156**, 94–105 (2019)
14. Yang, J., Chen, D., Kitipornchai, S.: Buckling and free vibration analyses of functionally graded graphene reinforced porous nanocomposite plates based on Chebyshev-Ritz method. Compos. Struct. **193**, 281–294 (2018)
15. Phung-Van, P., Nguyen-Xuan, H., Thai, C.H.: Nonlocal strain gradient analysis of FG GPLRC nanoscale plates based on isogeometric approach. Eng. Comput. **39**, 857–866 (2023)
16. Thai, C.H., Phung-Van, P.: A meshfree approach using naturally stabilized nodal integration for multilayer FG GPLRC complicated plate structures. Eng. Anal. Bound. Elem. **117**, 346–358 (2020)
17. Anamagh, M.R., Bediz, B.: Free vibration and buckling behavior of functionally graded porous plates reinforced by graphene platelets using spectral chebyshev approach. Compos. Struct. **253**, 112765 (2020)
18. MuniRami Reddy, R., Karunasena, W., Lokuge, W.: Free vibration of functionally graded-GPL reinforced composite plates with different boundary conditions. Aerosp. Sci. Technol. **78**, 147–156 (2018)
19. Ustundag, B.: On the free vibration behavior of cylindrical shell structures. Ph.D. thesis, Massachusetts Institute of Technology (2011)
20. Li, Z., et al.: Dynamic stiffness formulation for vibration analysis of an open cylindrical shell and its coupling structures based on a generalized superposition method. J. Sound Vib. **538**, 117237 (2022)
21. Safarpour, M., Rahimi, A., Alibeigloo, A.: Static and free vibration analysis of graphene platelets reinforced composite truncated conical shell, cylindrical shell, and annular plate using theory of elasticity and DQM. Mech. Based Des. Struct. Mach. **48**, 496–524 (2020)
22. Bidzard, A., Malekzadeh, P., Mohebpour, S.R.: Vibration of multilayer FG-GPLRC toroidal panels with elastically restrained against rotation edges. Thin-Walled Struct. **143**, 106209 (2019)
23. Nguyen, V.-L., Tran, M.-T., Limkatanyu, S., Mohammad-Sedighi, H., Rungamornrat, J.: Reddy's third-order shear deformation shell theory for free vibration analysis of rotating stiffened advanced nanocomposite toroidal shell segments in thermal environments. Acta Mech. **233**, 4659–4684 (2022)
24. Dat, N.D., Anh, V.T.T., Duc, N.D.: Vibration characteristics and shape optimization of FG-GPLRC cylindrical shell with magneto-electro-elastic face sheets. Acta Mech. **234**, 4749–4773 (2023)
25. Tao, Y., Chen, C., Kiani, Y.: Frequency analysis of smart sandwich cylindrical panels with nanocomposite core and piezoelectric face sheets. Acta Mech. **234**(8), 3219–3240 (2023)
26. Khodabakhsh, R., Saidi, A.R., Bahaadini, R.: Homotopy solution for nonlinear vibration analysis of multilayer graphene platelets-reinforced thin-walled pipes conveying fluid with rectangular cross-section. Acta Mech. **234**, 577–598 (2023)

27. Bidzard, A., Malekzadeh, P., Mohebpour, S.R.: A size-dependent nonlinear finite element free vibration analysis of multilayer FG-GPLRC toroidal micropanels in thermal environment. Compos. Struct. **279**, 114783 (2022)
28. Van Do, V.N., Lee, C.-H.: Static bending and free vibration analysis of multilayered composite cylindrical and spherical panels reinforced with graphene platelets by using isogeometric analysis method. Eng. Struct. **215**, 110682 (2020)
29. Van Do, V.N., Lee, C.-H.: Bézier extraction based isogeometric analysis for bending and free vibration behavior of multi-layered functionally graded composite cylindrical panels reinforced with graphene platelets. Int. J. Mech. Sci. **183**, 105744 (2020)
30. Mohammadi, H., Shojaee, M., Kiani, Y.: A simplified isogeometric approach for vibrational analysis of nanocomposite panels with a free-form curve. Thin-Walled Struct. **183**, 110426 (2023)
31. Abedini Baghbadorani, A., Kiani, Y.: Free vibration analysis of functionally graded cylindrical shells reinforced with graphene platelets. Compos. Struct. **276**, 114546 (2021)
32. Liu, D., Kitipornchai, S., Chen, W., Yang, J.: Three-dimensional buckling and free vibration analyses of initially stressed functionally graded graphene reinforced composite cylindrical shell. Compos. Struct. **189**, 560–569 (2018)
33. Qin, B., Wang, Q., Zhong, R., Zhao, X., Shuai, C.: A three-dimensional solution for free vibration of FGP-GPLRC cylindrical shells resting on elastic foundations: a comparative and parametric study. Int. J. Mech. Sci. **187**, 105896 (2020)
34. Wang, A., Chen, H., Hao, Y., Zhang, W.: Vibration and bending behavior of functionally graded nanocomposite doubly-curved shallow shells reinforced by graphene nanoplatelets. Results Phys. **9**, 550–559 (2018)
35. Esmaeili, H., Kiani, Y., Beni, Y.T.: Vibration characteristics of composite doubly curved shells reinforced with graphene platelets with arbitrary edge supports. Acta Mech. **233**, 665–683 (2022)
36. Qin, Z., Zhao, S., Pang, X., Safaei, B., Chu, F.: A unified solution for vibration analysis of laminated functionally graded shallow shells reinforced by graphene with general boundary conditions. Int. J. Mech. Sci. **170**, 105341 (2020)
37. Yee, K., Ghayesh, M.H.: A review on the mechanics of graphene nanoplatelets reinforced structures. Int. J. Eng. Sci. **186**, 103831 (2023)
38. Affdl, J.H., Kardos, J.: The Halpin-Tsai equations: a review. Polym. Eng. Sci. **16**, 344–352 (1976)
39. Reddy, J.N.: Theory and Analysis of Elastic Plates and Shells. CRC Press, Boca Raton (2006)
40. Sanders Jr, J.L.: An improved first-approximation theory for thin shells. NASA Rep. (1959)
41. Razgordanisharahi, A., Alipour Ghassabi, A., Hellmich, C.: Free vibration analysis of cylindrical honeycomb sandwich panels using state-space Levy method. Thin-Walled Struct. **182**, 110308 (2023)
42. Wang, C., Reddy, J.N., Lee, K.: Shear Deformable Beams and Plates: Relationships with Classical Solutions. Elsevier, Amsterdam (2000)
43. Patel, A., Das, R., Sahu, S.K.: Experimental and numerical study on free vibration of multiwall carbon nanotube reinforced composite plates. Int. J. Struct. Stab. Dyn. **20**, 2050129 (2020)